Regular Article

PHYSICAL CHEMISTRY RESEARCH
Published by the
Iranian Chemical Society
www.physchemres.org
info@physchemres.org

Phys. Chem. Res., Vol. 10, No. 3, 325-331, September 2022
DOI: 10.22036/PCR.2021.300339.1970

Dielectric Properties of Ultra-Low Dielectric Constant PVA-Pentaerythritol/MnO_2 Nanocomposite

S.H. Merza[a,*] and E. Fadil Mousa[b]

[a]*Depratment of Chemistry, College of Education for Pure Science (Ibn Al-Haitham), University of Baghdad, Baghdad, Iraq*
[b]*Department of Chemistry, College of Science for Women, University of Baghdad, Baghdad, Iraq*
(Received 22 September 2021, Accepted 26 November 2021)

In this work, a simple method was used to prepare the MnO_2 nanoparticles. These nanoparticles then were characterized by several techniques, such as X-ray diffraction, Fourier transform infrared spectroscopy, scanning electron microscopy (SEM) and atomic force microscope (AFM). The results showed that the diffraction peak of MnO_2 nanoparticles was similar to that of standard data. The images of AFM and SEM indicated that the MnO_2 nanorods were growing from the MnO_2 nano spherical shape. PVA-pentaerythritol/MnO_2 nanocomposite films were fabricated by evaporating casting method. The dielectric constant and loss tangent of P-Ery/MnO_2 films were measured between 10 kHz and 1 MHz using LCR. As the content of MnO_2 increased, the dielectric constant decreased from 1.6 to 1.3. The loss tangent of P-Ery was very low at 400 kHz, which increased by an increase in the MnO_2 content. Thermogravimetric analysis and Scanning electron microscope methods were used to investigate the thermal stability and surface analysis of the films.

Keywords: Loss tangent, Clausius-Mossotti equation, MnO_2 nanorod, Scanning electron microscopy (SEM), X-ray diffraction (XRD)

INTRODUCTION

Materials with low dielectric constant were developed to replace the silicon dioxide as interlevel dielectrics [1]. These materials show great application in the fields of semiconductor packaging, interlayer dielectric, electronic and communication devices. A potential problem in this field is resistance-capacitance delays, cross-talk noise, and excessive power dissipation [2,3]. Therefore, researchers have used materials having more insulating and low dielectric constant (≤ 2.5 or ultra-low ≤ 2.0) [4-7].

Generally, according to the Clausius-Mossotti equation [8], various approaches have been devised to design insulating polymer materials and materials with reduced dielectric constant value. The former is the materials that have low electric dipole chemical bonds such as alicyclic groups, fluorinated groups, or those that introduce large molar bulk such as fluorine, phenyl, and biphenyl to the molecular design [9]. The second one is the materials which can reduce the total number density of dipoles by effectively rearranging the material structure or increasing the free volume [10,11]. The incorporation of nanometer-sized pores within the polymer matrix also can reduce the dielectric constant value. Porosity may be introduced within a material without any treatment (constitutive porosity) or by adding an ingredient or selective etching (subtractive porosity).

Several researches have been focused on synthesis of novel class of materials, organic and inorganic composites with low dielectric constant such as silica, doping silica, organic polymeric materials, and silsesquioxane [2]. For example, Yiwu *et al*. has reported a new polyimide with the lowest dielectric constant (ε') of 1.52 at 10 kHz and with a glass-transition temperature (Tg) of 280 °C [12]. Yang et al. has developed a novel class of organosilicates from sets of triblock polymers, poly (ethylene oxide-b-propylene oxide-b-ethylene oxide) as sacrificial materials in poly (methyl silsesquioxane) with an ultra-low-dielectric

*Corresponding author. E-mail: sundusm.sm@gmail.com

constant of less than 2.0 [13]. Silica/polyimide (SiO_2/PI) composite nanofiber membrane using two approaches sol-gel and electrospinning was prepared by Leipeng *et al.* The dielectric constant of the composite membranes changed in the range of 1.78 to 1.32 with increasing the content of SiO_2. The thermal stability of PI increased after mixing with SiO_2 [14]. Zhang *et al.* have also incorporated nano-fillers into the PI matrix to obtain a composite with a low dielectric constant of 2.8 [15]. Abdulwahhab *et al*. prepared and studied electrical and dielectric properties of ternary hybrid nanocomposite: reduced graphene oxide, MnO_2 nanorod, and poly (anthranilic acid) embedded in poly (vinyl alcohol). The dielectric constant and the loss tangent (tan δ) for nanocomposite were in the range of 1.42 to 2.06 and 0.2 to 0.41 at frequencies of 2 MHz and 10 kHz, respectively [16].

In this work, a new ploy (vinyl alcohol) (P)-pentaerythritol (Ery)/MnO_2 composite with ultralow dielectric constant was fabricated by a simple solution mixing. Dielectrical and thermal properties were used to characterize the dielectric films.

EXPERIMENTAL

Materials

Ploy (vinyl alcohol) is fully hydrolyzed from SIGMA**.** Pentaerythritol and all other chemicals were analytical grade and provided from Fluka.

Preparation of MnO_2 Nanoparticles

MnO_2 nanoparticles were synthesized according to the references [17,18] where 0.3 M $KMnO_4$ was added with spray technique to 1.9 M $MnSO_4$. HNO_3 was added to adjust pH at 1 and the reaction was refluxed at 60-100 °C for 8 h. The mixture was ultrasonicated for one hour .The product was filtered, rinsed and dried in vacuum at 100 °C for 2 h. MnO_2 nanoparticles were synthesized according to Eq.(1)

$$MnO^{-}_{4\,(aq)} + 4H^{+}{}_{(aq)} + 3e^{-} \rightarrow MnO_{2(s)} + 2H_2O \quad (1)$$

Preparation of P-Ery/MnO_2 Nanocomposite

5 g Ploy (vinyl alcohol) was dissolved in 100 ml deionized water at 90 °C for 1 h, the solution then cooled to R.T. Appropriate weight of pentaerythritol was added to 10 ml of 5% ploy (vinyl alcohol) solution with ultrasonicated using probe sonication to prepare ratio of ploy (vinyl alcohol)/pentaerythritol blend (P-Ery) (90:10) which has good transparency. Different weights of MnO_2 nanoparticles (0.03, 0.05, 0.08, and 0.11%) were added to 10 ml (P-Ery) blend with ultrasonic for one hour until a homogeneous solution was obtained. The P-Ery/MnO_2 nanocomposite was fabricated by evaporating casting method. The solution poured into a clean square glass (dimension 2.5 × 3 cm) and kept at R.T for one day. After drying the films pull off.

Characterization

Dielectric performances of prepared nanocomposite were investigated using a precision LCR meter (8101G) with a frequency range of 10 kHz to 1 MHz. Scanning electron microscopy (Zeiss) (Germany) (SEM) and atomic force microscopy compact (AFM) PHYWE (Germany) were used to find out the morphology of the P-Ery, P-Ery/MnO_2 nanocomposite and MnO_2 nanoparticles. The thermal properties were estimated by thermal gravimetric analysis TGA (Universal V4.5A TA Instruments) under air atmosphere with heating rate of 10 °C min^{-1}. Also, X-ray diffraction (XRD) 6000 Shimadzu (Japan) with an incident Cu-Kα (λ = 1.54 Å), 30 mA and 40.0 kV; scan range (2θ = 5-80°), and scan speed (10 deg min^{-1}) was applied. FT-IR spectrophotometer, Shimadzu, 8400s, (Japan) was used.

RESULT AND DISCUSSION

AFM and SEM of MnO_2 Nanoparticles

Figure 1A shows the two dimension histogram of the growth of spherical MnO_2 nanoparticles with length of 127.1 nm. Figure 1B shows the cross section of MnO_2; their typical diameter and particle size was 5.48, 12.48 nm, respectively. Figure 1C shows a SEM image of the growth MnO_2 nanorods with highly accumulation as shown in arrows.

FT-IR of MnO_2 Nanoparticles

The FT-IR spectrum of MnO_2 nanoparticles is presented

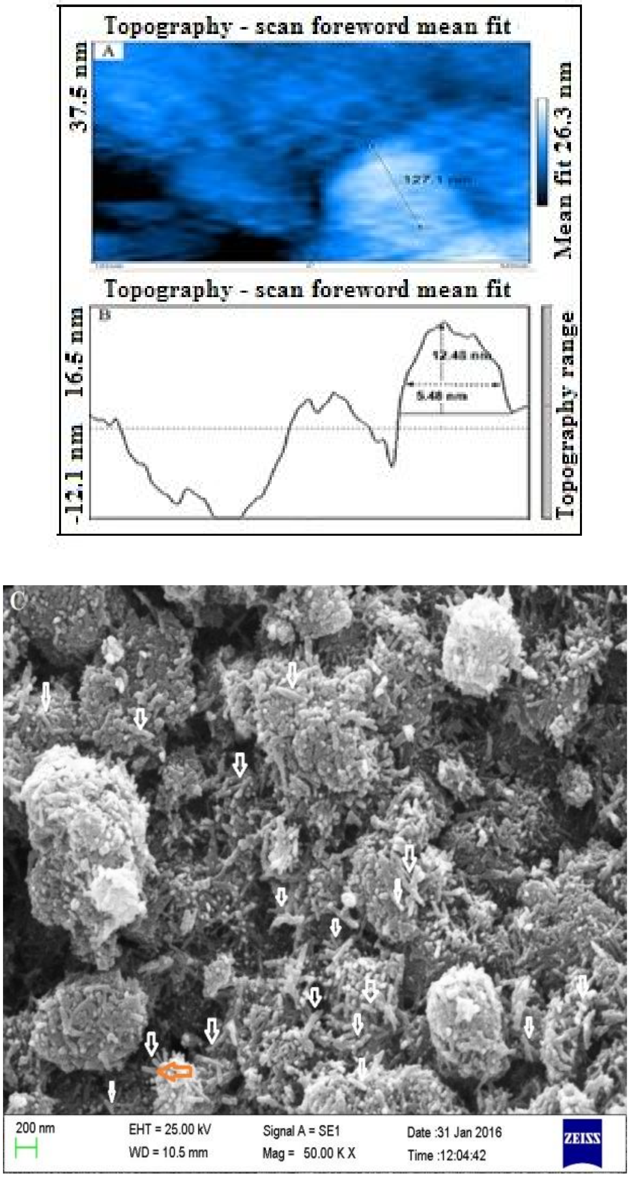

Fig. 1. AFM images of MnO_2 nanoparticles (A) 2 D (B) cross-section (C) SEM image of MnO_2 nanoparticles with 200 nm magnification.

in Fig. 2. The graph gives absorption peaks of Mn-O bond at 526 cm^{-1} and 480 cm^{-1} [19]. The peak at 716 cm^{-1} assigned to the stretching mode of MnO_6 octahedral along the double chain [20,21]. These peaks confirm that the α-MnO_2 was obtained. The peak at 3383 cm^{-1} can be attributed to the vibrations of adsorbed water molecules.

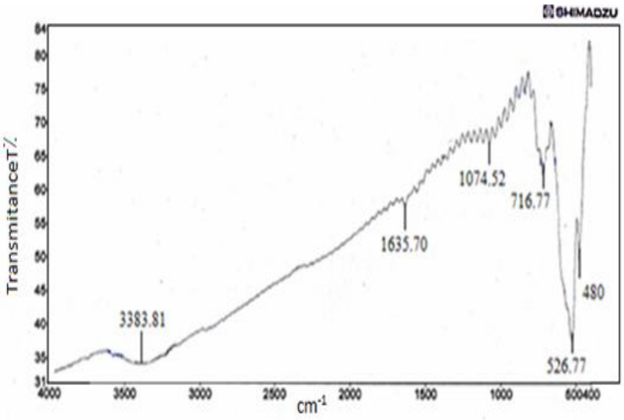

Fig. 2. FT-IR Spectrum of MnO_2 nanopatricles.

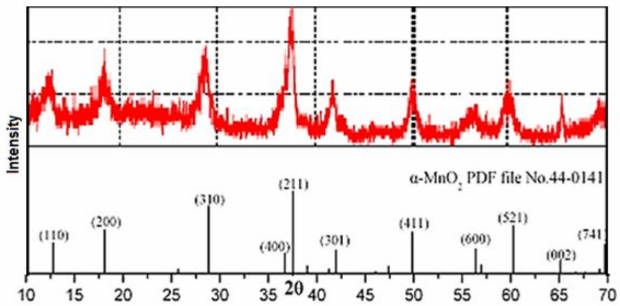

Fig. 3. X-ray Diffraction pattern of as-synthesized MnO_2 nanoparticles.

The bands at 1635 cm^{-1} and 1074 cm^{-1} are related to the O-H bending vibration.

XRD of MnO_2 Nanoparticles

The XRD powder pattern of MnO_2 was presented in Fig. 3. The diffraction peaks at 2θ = 12.69, 18.1, 28.75, 37.5, 42.02, 49.8, 56.4, and 60.09 are attributed to the crystal planes of α-MnO_2 (JCPDS card No.44-0141) [22]. The mean size (t) of MnO_2 nanoparticles was estimated from Debye-Scherer's formula Eq. (2) and calculated as 11.8 nm using the strongest diffraction peak of (211)

$$t = \lambda \frac{k}{\beta \cos\theta} \tag{2}$$

Where k is the Scherer constant (0.9), (λ = 0.1541 nm) for Cu Kα radiation source, β is the angular full width at half maximum peak (FWHM) intensity in radian, and θ is the Bragg angle (deg). No peaks of other phases were detected that indicated a high purity of the synthesized product.

Dielectrical Properties

The dielectric constant (ε') of the P-Ery and P-Ery/MnO_2 nanocomposite films were calculated by using capacitance measurement *via* the following formulation:

$$\varepsilon' = \frac{cd}{\varepsilon^{\circ} A} \qquad (3)$$

Where (c), (ε°), (d), and (A) are the capacitance in Farad (F), permittivity of free space (8.854 × 10^{-12}) F.m^{-1}, thickness of the sample (m), and the area of the electrode (m^2), respectively. The thickness of films was measured using vernier caliper in range of (0.2 × 10^{-3}-0.35 × 10^{-3}) m^2 and the electrode area used in this investigation was 1.32 × 10^{-4} m^2. The respective plot of dielectric constant and loss tangent of P-Ery blend and P-Ery/MnO_2 nanocomposite as function of frequency (10 kHz-1 MHz) is shown in Fig. 4. As shown in this Figure, the dielectric constant of P-Ery (90:10) blend has low values from 1.65 to 1.59 within the range of frequencies. This may be due to the presence of bulky and pendant OH groups of pentaerythritol, which have limit chain packing density and limit movement of freedom chain. By increasing the MnO_2 content, the dielectric constant of P-Ery/MnO_2 nanocomposite was decreased to ultralow value of 1.11 at 1 MHz; this may be due to the rearrangement of the structure of P-Ery blend *via* forming the constitutive voids and tight interface between MnO_2 NPs and P-Ery matrix.

In interlayered packaging and related applications, the loss tangent (tan δ) or dissipation factor is a critical parameter to determine the dissipation of heat energy of dielectric material. The loss tangent was determined using the equation below:

$$\tan\delta = \varepsilon'' / \varepsilon' \qquad (4)$$

In above equation, (ε") is the imaginary part. Figure 4 shows the loss tangent of P-Ery and P-Ery/MnO_2 composite. At the frequency of 400 kHz, the dielectric losses of P-Ery with different content of MnO_2 were 0.029, 0.013, 0.011, and 0.012. As MnO_2 content increases, the absence of the interfacial defects and polarization due to the compatibility between MnO_2 and P-Ery composite possibly results in a low loss tangent. The dielectric loss of P-Ery was very low, lower than the values reported in literature [14,16], which was sufficient for practical applications. The values of tan δ of P-Ery and P-Ery/MnO_2 nanocomposite films at 10 kHz, 400 kHz, and 1 MHz are summarized in Table 1.

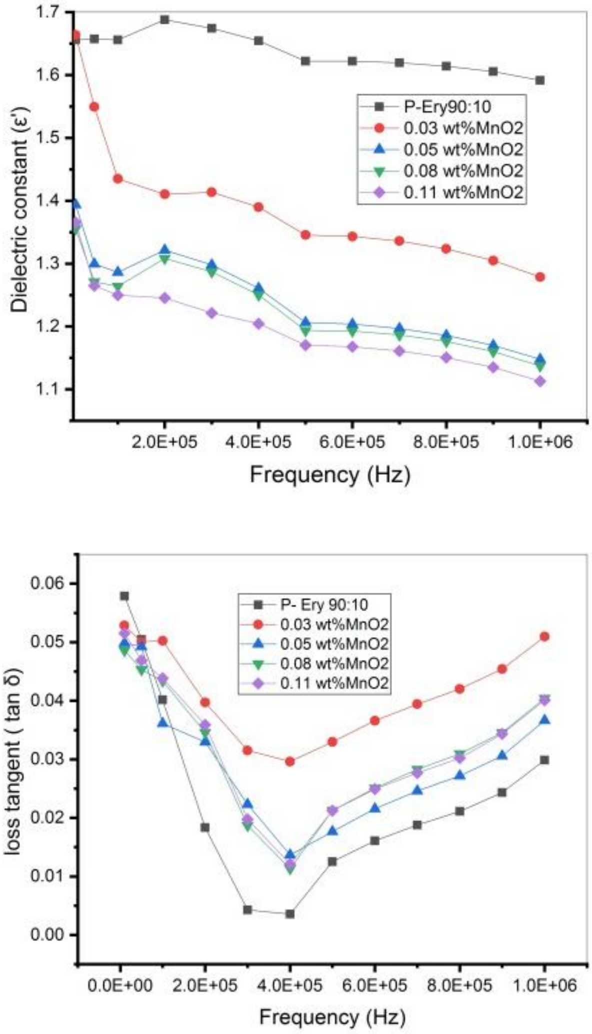

Fig. 4. Dielectric constant and loss tangent of P-Ery and P-Ery/MnO_2 nanocomposite with different concentration of MnO_2.

Table 1. Values of Loss Tangent of P-Ery and P-Ery/MnO_2 Composite at 10 kHz, 400 kHz and 1 MHz

Samples	10 kHz	400 kHz	1 MHz
P-Ery	0.057	0.003	0.029
P-Ery/MnO_2 (0.03) wt%	0.052	0.029	0.050
P-Ery/MnO_2 (0.05) wt%	0.049	0.013	0.036
P-Ery/MnO_2 (0.09) wt%	0.048	0.011	0.040
P-Ery/MnO_2 (0.11) wt%	0.051	0.012	0.040

Morphology of P-Ery and P-Ery/MnO_2 Films

SEM was carried out to investigate the surface analysis and effect of dispersion of MnO_2 in P-Ery matrix. As shown in Fig. 5, the surface of the P-Ery and P-Ery/MnO_2 (0.03) wt% nanocomposite were observed to be relatively rough. At higher content of MnO_2, SEM image shows formed adventitious pores which were the essential reason for diminishing dielectric constant [9]. Also the dispersion of MnO_2 in the P-Ery matrix was homogeneous demonstrating good compatibility and good interaction between MnO_2 NPs and P-Ery matrix.

Thermal Properties of P-Ery and P-Ery/MnO_2 Films

TGA was used to deduce the thermal stability of P-Ery and P-Ery/MnO_2 films. It shows the alteration in mass of a sample as a function of temperature in atmospheric conditions. The details of TGA data for P-Ery and P-Ery/MnO_2 films are presented in Table 2. It can be seen from the table that the main thermal decomposition of P-Ery

Table 2. TGA Data of Samples

Sample	Weight loss (%)	Temperature (°C)
P-Ery	3.57	150
	70.66	410
P-Ery/MnO_2	4.42	201
(0.03) wt%	76.20	400
P-Ery/MnO_2	5.19	201
(0.11) wt%	69.05	395

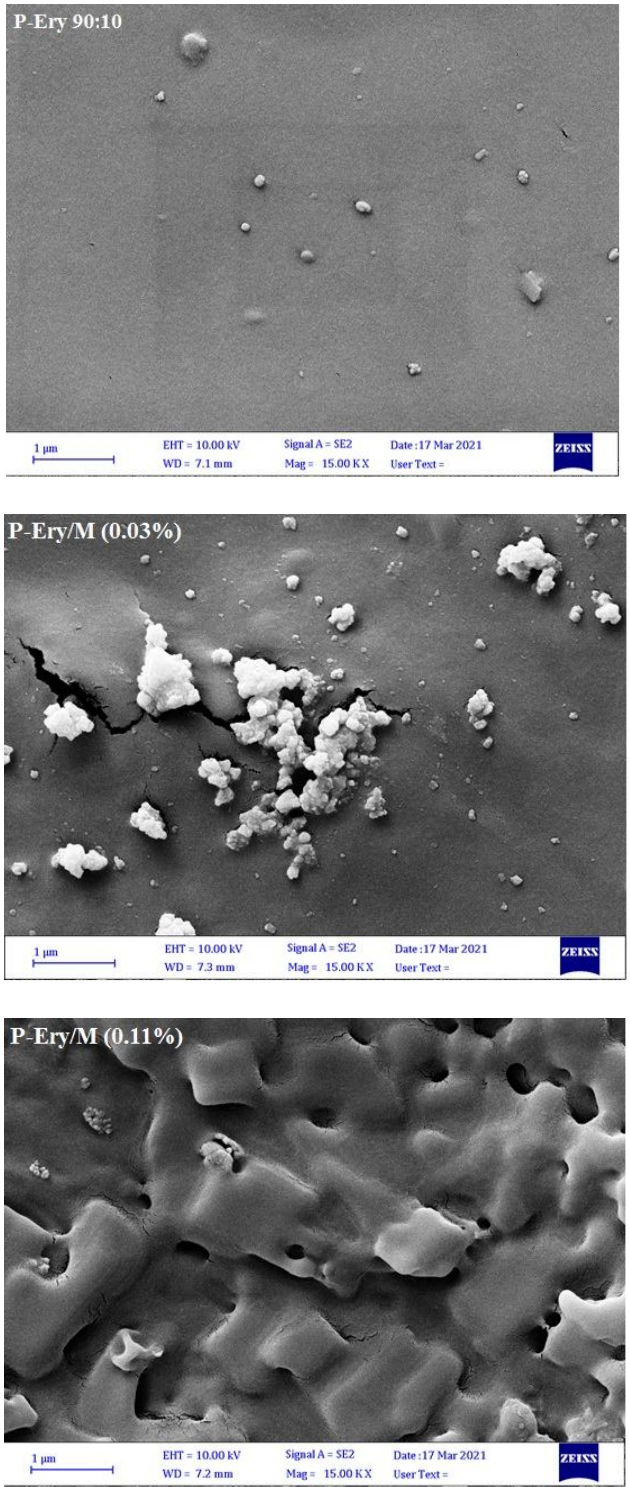

Fig. 5. Morphology of P-Ery and P-Ery with different content of MnO_2.

started at 150 °C and the temperatures of the main thermal decomposition film samples shifted to the higher temperature region (200 °C) with the addition of MnO_2 °C. The temperature of maximum rate of P-Ery, P-Ery/MnO_2 (0.03) wt%, and P-Ery/MnO_2 (0.11) wt% samples were found to be 410, 400, and 395 °C, respectively.

CONCLUSIONS

In this work, a series of P-Ery and P-Ery/MnO_2 composites were fabricated. The dielectric constant was reduced to 1.1 at 1 MHz by an increase in the content of MnO_2 at room temperature. Further investigation of the dielectric properties of composites has shown low dielectric loss of < 0.029 at 400 KHz. The thermal stability was studied by TGA. The result showed that the P-Ery/0.03 wt% MnO_2 nanocomposite had good thermal stability with 4.42 wt% loss temperature of 201 °C and a residual of 76.20% at 400 °C. The incorporation of MnO_2 nanoparticles results in a good dielectric providing characteristics for high-performance electronics.

ACKNOWLEDGEMENTS

The authors are grateful for the support from department of chemistry/college of education for pure science (Ibn Al-Haitham)/University of Baghdad.

REFERENCES

[1] Morgen, M.; Ryan, E. T.; Zhao, J. H.; Hu, C.; Cho, T. H.; Ho, P. S., Low dielectric constant materials for ULSI interconnect, *Annu. Rev. Mater. Sci.* **2000**, *30*, 645-680, DOI: 10.1146/annurev.matsci.30.1.645.

[2] Volksen, W.; Miller, R. D.; Dubois, G., Low dielectric constant materials. *Chem. Rev.* **2010**, *110*, 56-110, DOI: 10.1021/cr9002819.

[3] Shamiryan, D.; Abell, T.; Iacopi, F.; Maex, K., Low-k dielectric materials. *Mater. Today*. **2004**, *7*, 34-39, DOI: 10.1016/S1369-7021(04)00053-7.

[4] Miller, R. D., In Search of low-k dielectrics. *Science*. **1999**, *286*, 421-422, DOI: 10.1126/ science.286.5439.421.

[5] Grill, A.; Gates, S. M.; Ryan, T. E.; Nguyen, S. V.; Priyadarshini, D., Progress in the development and understanding of advanced low k and ultralow k dielectrics for very large-scale integrated interconnects State of the art. *Appl. Phys. Rev.* **2014**, *1*, 011306, DOI: 10.1063/1.4861876.

[6] Maier, G., Low dielectric constant polymers for microelectronics. *Prog. Polym. Sci.* **2001**, *26*, 3-65, DOI: 10.1016/S0079-6700(00)00043-5.

[7] Farrell, R.; Goshal, T.; Cvelbar, U.; Petkov, N.; Morris, M. A., Advances in ultra-low dielectric constant ordered porous materials. *Electrochem. Soc. Interface.* 2011, *20*, 39-46, DOI: 10.1149/2.F04114if.

[8] Kurinchyselvan, S.; Sasikumar, R.; Ariraman, M.; *et al.,* Low dielectric behavior of amine functionalized MCM-41 reinforced polyimide nanocomposites. *High Perform. Polym*. **2015**, *28*, 842-853, DOI: 10.1177/ 0954008315604035.

[9] Jingting, W.; Yanfeng, W.; Xuesong, L.; Jianxin, M., Ultra-low dielectric constant materials with hydrophobic property: Synthesis of poly (aryl ether sulfone) with POSS and biphenyl group in the main chain. *High Perform. Polym.* **2019**, *31*, 503-512, DOI: 10.1177/ 0954008318789462.

[10] Liaw, D. J.; Wang, K. L.; Huang, Y. C.; Lee, K. R.; Lai, J. Y.; Ha, C. S., Advanced polyimide materials: Syntheses, physical properties and applications. *Prog. Polym. Sci.* **2012**, *37*, 907-974, DOI: 10.1016/ J.PROGPOLYMSCI.2012.02.005.

[11] Liu, Y. W.; Zhang, Y.; Lan, Q.; Liu, S. W.; Qin, Z. X.; Chen, L. H.; Zhao, C. Y.; Chi, Z. G.; Xu, J. R.; Economy, J., High-performance functional polyimides containing rigid nonplanar conjugated triphenylethylene moieties. *Chem. Mater*. **2012**, *24*, 1212-1222, DOI: 10.1021/cm3003172.

[12] Yiwu, L.; Chao Q.; Lunjun, Q.; Yunan, W.; Yi, Zh.; Xinhui, W.; Bing, Z.; Wenxin, Ch.; Zhiquan, Ch.; Zhenguo, Ch.; Siwei, L.; Xudong, Ch.; Jiarui, X., A bulk dielectric polymer film with intrinsic ultralow dielectric constant and outstanding comprehensive properties. *Chem. Mater.* **2015**, *27*, 19, 6543-6549, DOI: 10.1021/acs.chemmater.5b01798.

[13] Yang, S.; Pai, C.; Nalamasu, O.; Reichmanis, E.; Mirau, P.; Obeng, Y.; Seputro, J.; Lin, E.; Lee, V., Design of a nanoporous ultra low-dielectric constant

organosilicate. International Conference on Polymers in Electronic Packaging. **2001**, *42* (1).

[14] Leipeng, L.; Fengzhu, L.; Penggang, L.; Ling, D.; Wangshu, T.; Paul, K. Ch.; Yihe, Zh., Preparation of ultra-low dielectric constant silica/polyimide nanofiber membranes by electrospinning. *Composites*. **2016**, Part A *84*, 292-298, DOI: 10.1016/ j.compositesa.2016.02.002.

[15] Zhang, Y. H.; Lu, S. G.; Li, Y. Q.; Dang, Z. M.; Xin, J. H.; Fu, S. Y., *et al*., Novel silica tube/polyimide composite films with variable low dielectric constant. *Adv. Mater*. **2005**, *17*, 1056-9, DOI: 10.1002/adma.200401330.

[16] Abdulwahhab, H. M.; Emaad, T. B.; Dhia, H. H., Dielectric properties of synthesized ternary hybrid nanocomposite embedded in poly (vinyl alcohol) matrix films. *Polym. Polym. Compos.* **2020**, *29*, 1-12, DOI: 10.1177/0967391120951406.

[17] Deguzman, R. N.; Shen, Y. F.; Neth, E. J., Synthesis and characterization of octahedral molecular sieves (OMS-2) having the hollandite structure. *Chem. Mater.* **1994**, *6*, 815-821, DOI: 10.1021/cm00042a019.

[18] Suh C. P.; Suk, F. Ch.; Chian Y. L., Controlled synthesis of manganese dioxide nanostructures *via* a facile hydrothermal route. *J. Nanomater.* **2012**, *2012*, 1-7, DOI: 10.1155/2012/607870.

[19] Khitam, S. Sh., Synthesis and characterization nano structure of MnO_2 *via* chemical method. *ETJ.* **2018**, *36*, 946-950, DOI: 10.30684/etj.36.9A.1.

[20] Kang, L.; Zhang, M.; Liu, Z. H.; Ooi, K., IR spectra of manganese oxides with either layered or tunnel structures. *Spectrochim. Acta. A.* **2007**, *67*, 864, DOI: 10.1016/j.saa.2006.09.001.

[21] Gotic, M.; Jurkin, T.; Music, S.; Unfried, K.; Sydlik, U., Bauer-Šegvic, microstructural characterizations of different Mn-oxide nanoparticles used as models in toxicity studies. *J. Mol. Struct. A* **2013**, *10*, 248-254, DOI: 10.1016/j.molstruc.2012.09.083.

[22] Feng, L.; Xuan, Zh.; Zhao, H.; Bai, Y.; Guo, J.; Su, C. W.; Chen, X., MnO_2 prepared by hydrothermal method and electrochemical performance as anode for lithium-ion battery. *Nanoscale Res. Lett.* **2014**, *9*, 290, DOI: 10.1186/1556-276X-9-290.